Chapter

Dusty Plasmas in Supercritical Carbon Dioxide

Yasuhito Matsubayashi, Noritaka Sakakibara, Tsuyohito Ito and Kazuo Terashima

Abstract

Dusty plasmas, which are systems comprising plasmas and dust particles, have emerged in various fields such as astrophysics and semiconductor processes. The fine particles possibly form ordered structures, namely, plasma crystals, which have been extensively studied as a model to observe statistical phenomena. However, the structures of the plasma crystals in ground-based experiments are two-dimensional (2D) because of the anisotropy induced by gravity. Microgravity experiments successfully provided opportunities to observe the novel phenomena hidden by gravity. The dusty plasmas generated in supercritical fluids (SCFs) are proposed herein as a means for realizing a pseudo-microgravity environment for plasma crystals. SCF has a high and controllable density; therefore, the particles in SCF can experience pseudo-microgravity conditions with the aid of buoyancy. In this chapter, a study on the particle charging and the formation of the plasma crystals in supercritical CO_2, the realization of a pseudo-microgravity environment, and the outlook for the dusty plasmas in SCF are introduced. Our studies on dusty plasmas in SCF not only provide the pseudo-microgravity conditions but also open a novel field of strongly coupled plasmas because of the properties of media.

Keywords: plasma crystal, supercritical fluid, pseudo-microgravity, surface dielectric barrier discharge, dusty plasmas in dense fluids

1. Introduction

The dynamics of statistical phenomena, such as phase transitions and wave propagation, and kinetic phenomena, such as the motion of dislocations in a crystal, are difficult to observe because atoms are too small. For a long time, many models have been developed that imitate crystal structures and can be observed with an optical microscope. For example, in 1947, Bragg, who established X-ray diffraction, and Nye reported the bubble model to understand the dynamics of dislocations [1]. The most extensively studied system is probably a charged particle system. For example, colloidal crystals, ordered structures of microparticles in colloidal dispersion, were developed [2]. Colloidal crystals have been studied not only as a model of crystal structure but also for application to optical materials [3]. Interparticle distances are close to the wavelength of visible light, which results in opalescence.

Dusty plasmas or fine particle plasmas, a system composed of dust particles and plasmas, have also been extensively studied as a model of crystal structure. In 1986,

Ikezi theoretically predicted that microparticles (diameter, 0.3–30 μm) embedded in a commonly used plasma processing possibly form an ordered structure or plasma crystal [4]. Microparticles inside the plasma become negatively charged because of the higher mobility of electrons. The charged particles exert a repulsive Coulombic force on each other. Plasma crystals can be formed when the interparticle electrostatic potential exceeds the kinetic energy of particles. A good measure for the formation of plasma crystals is a Coulomb coupling parameter Γ. Γ is defined as a ratio of the electrostatic potential energy to the kinetic energy of particles. The plasma with $\Gamma > 1$ is defined as a strongly coupled plasma [5], and Monte Carlo simulation suggests that an ordered structure can be formed when $\Gamma > 170$ [6].

In 1994, three independent groups simultaneously reported the experimental observation of plasma crystals [7–9]. However, these crystal structures were strongly affected by gravity. Because the electric field in a plasma sheath can compensate for gravity, the structure of plasma crystals can be maintained in a sheath region. Such compression in a direction of gravitational force gives plasma crystals a two-dimensional (2D) structure. To eliminate the gravitational anisotropy, microgravity experiments using the International Space Station and a sounding rocket have been conducted and provided three-dimensional (3D) plasma crystals [10]. The 3D plasma crystals in microgravity experiments show some new phenomena, such as an unexpected void structure and various crystal structures (fcc, bcc, and hcp) [11]. Such microgravity experiments give promising results; however, they are time-consuming and costly. To overcome the time and cost issues, a ground-based "microgravity" experiment is greatly needed. Previously, several concepts have been proposed. Applying thermophoretic force was reported as an effective approach to cancel gravity [12, 13]. The shell structure of dust particles, "Coulomb balls," was found. Another approach is the magnetic field. It was reported that the magnetic field applied on super-paramagnetic particles can compensate for the gravity [14]. In the case of colloidal dispersion, gravity affects the crystal structures in a similar manner. Microgravity experiments were conducted as is for dusty plasmas, which revealed that the crystal structure under microgravity is basically random stacking of hexagonally close-packed planes alone and suggested that fcc, which is often observed in ground-based experiments, is induced by gravity [15]. Buoyancy is employed to compensate for gravity in ground-based experiments [16]. Buoyancy can be tuned by changing the ratio of H_2O and D_2O; the density of media can be matched to that of microparticles.

In the present study, buoyancy in supercritical fluids (SCFs) is proposed as a means for compensating for gravity in dusty plasmas. SCF is a state of matter whose temperature and pressure exceed those of the critical point (T_c, P_c), as described in **Figure 1**. The critical point is the end point of the vapor pressure curve, above which it is impossible to distinguish whether the phase is gas or liquid, and the phase is defined as SCF. SCF has liquid-like solubility, high density, and gas-like low viscosity. Owing to such unique properties, SCF has been applied to fabrication processes of such materials as aerogels and nanoparticles [17]. The critical temperature T_c varies with molecules. CO_2 and Xe are frequently used as SCF media, because they have T_c near room temperature, 304 and 290 K, respectively. The critical pressure P_c of each medium is 7.38 and 5.84 MPa, respectively; therefore, temperature control by a water cooling/heating system, and the application of pressure by a pump can provide SCF states of CO_2 and Xe. The properties of SCF that are significant for the application to dusty plasmas are density and viscosity. **Figure 2a** shows the dependence of the density of CO_2, Xe, and typical liquid (H_2O and ethanol) on pressure. The temperatures of Xe and CO_2 are their own T_c, and those of water and ethanol are set to room temperature (293 K). The densities of H_2O and ethanol show little change against pressure. Meanwhile, those of CO_2 and

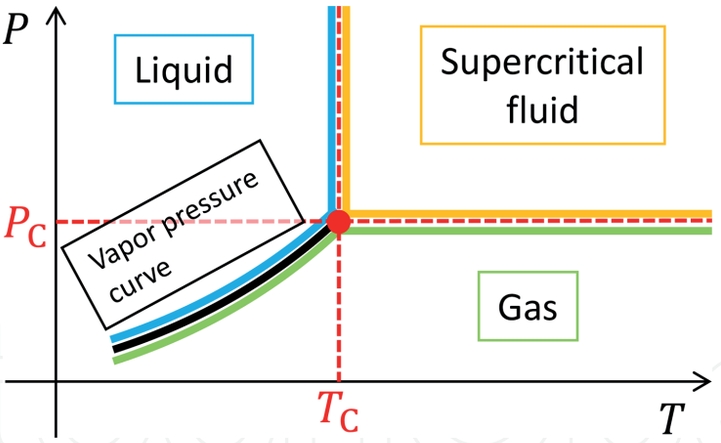

Figure 1.
T-P *phase diagram of a matter focusing around the critical point.*

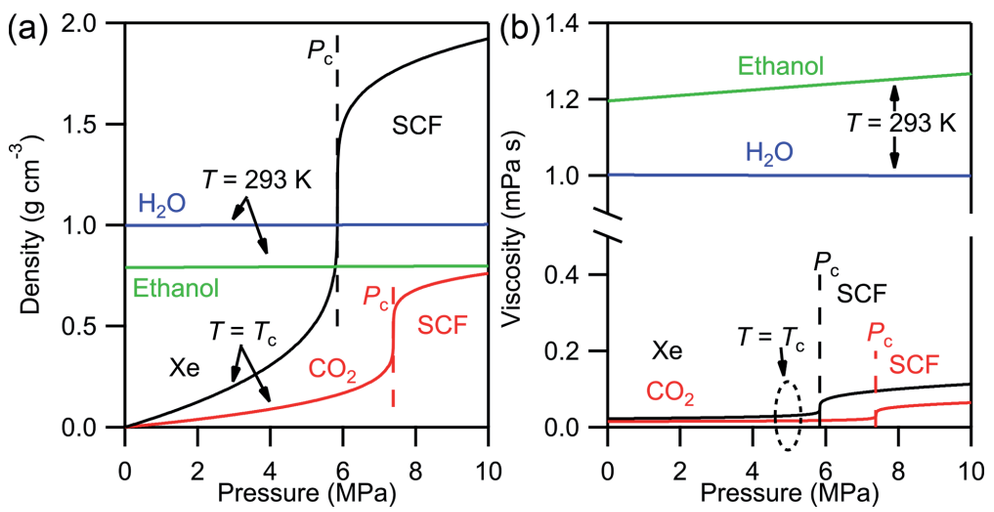

Figure 2.
Dependences of the density (a) and the viscosity (b) of Xe, CO_2, H_2O, and ethanol on pressure: the temperatures of the former two and the latter two are set to their own T_c and room temperature (293 K), respectively (the values were obtained from the NIST database [25]).

Xe successively increase with increasing pressure and reach or exceed those of typical liquids above P_c, where they become SCF. This means that controllable buoyancy can be applied to microparticles in SCF, which possibly results in the realization of pseudo-microgravity conditions for dusty plasmas. **Figure 2b** shows the dependence of the viscosity of each medium on pressure. Despite the large density of SCF, the viscosities are only one-tenth those of typical liquids. Therefore, microparticles in SCF experience little viscous drag, which delays reaching a condition of thermal equilibrium, as is observed in colloidal dispersion [19]. Therefore, SCFs are considered to be attractive media suitable for the generation of dusty plasmas in a pseudo-microgravity condition.

The generation of nonthermal plasmas in SCF is challenging, because the pressure is so high that applying higher voltage is necessary based on Paschen's law. The discharge plasmas in SCFs have been successfully generated by employing electrodes with a gap on the order of micrometers [20]. The possibilities of the plasmas in SCF for application to carbon nanomaterial syntheses and unique phenomena, such as a large decrease of breakdown voltage near the critical point, were shown [21]. For application to the generation of dusty plasmas, surface dielectric barrier discharge (DBD) in the field-emitting regime was employed [22]. The breakdown voltages of CO_2 for the discharges in the "standard regime," in which electrons are

dominantly provided by ionizations, increase with increasing pressure, while it was found that field emission plays a major role in generating discharges under high pressure, which results in discharges with breakdown voltages as low as 2 kV. The surface DBD in the field-emitting regime is considered to be suitable for the generation of dusty plasmas in SCF, because the discharge with such low breakdown voltages possibly generates less heat and causes less damage to microparticles and electrodes.

In this chapter, a study on dusty plasmas in supercritical CO_2 ($scCO_2$) is introduced. In Section 2, the first report on the generation of dusty plasmas in SCF, on the formation of plasma crystals in $scCO_2$, and on the estimation of the particle charges is described [23]. Section 3 covers the realization of a pseudo-microgravity environment for dusty plasmas in $scCO_2$ and the 3D arrangement of particles [24]. In Section 4, the outlook for dusty plasmas in SCF, which includes the further applications of pseudo-microgravity conditions and the comparisons with other strongly coupled plasmas, is briefly discussed.

2. Motion of particles in dusty plasmas generated in $scCO_2$

The particle motion in dusty plasmas generated in $scCO_2$ was analyzed. The particles were electrically charged by the surface DBD in the field-emitting regime and showed the formation of an ordered structure above the electrodes. The analysis of the equation of motion revealed that the charge of a particle was on the order of -10^4 to $-10^5 e$ C (e: elementary charge). The kinetic energy of a particle was estimated by recording the motion with a high-speed camera. The estimated Coulomb coupling parameter was 10^2–10^4, from which the formation of strongly coupled plasmas was confirmed.

2.1 Experimental approach

Figure 3 shows a schematic diagram of the experimental setup for the generation of the dusty plasmas in $scCO_2$. As shown in **Figure 3a**, CO_2 pressurized by a high-pressure pump with a cooling circuit was introduced into the high-pressure chamber. The temperature inside the chamber was controlled by a water cooling/heating system. The temperature and pressure of CO_2 were 304.1–305.8 K and 0.10–8.33 MPa, respectively, which includes gaseous, liquid, and SCF states of CO_2. High voltages of up to 10 $kV_{p\text{-}p}$ with a frequency of 0.1–10 kHz were applied to the electrode. The microparticles (divinylbenzene resin; diameter, 30.0 μm; density, 1.19 g cm^{-3}) were placed on the etched region of the electrodes before applying voltages. The density of the particles was larger than that of CO_2 in this experimental condition; therefore, a pseudo-microgravity condition could not be achieved. The interest of this study is the charging and the motion of the particles in $scCO_2$. The motion of microparticles was observed by an optical microscope through a sapphire window under light-emitting diode (LED) illumination, as shown in **Figure 3b**. The high-speed camera was employed for the detection of the fast motion with frame rates up to 1000 fps. The motion in the direction of gravitational force was observed through a mirror. **Figure 3c** shows the detailed structure of the electrodes. The upper, powered electrode consists of a Cu film deposited on polyimide film, etched in a linear fashion, and closed by Ag pastes to confine particles. This rectangular region is referred to as the "etched region." The thicknesses of the Cu films and polyimide films were 30 and 20 μm, respectively. Ag paste was deposited on the reverse side and connected to the grounded chamber.

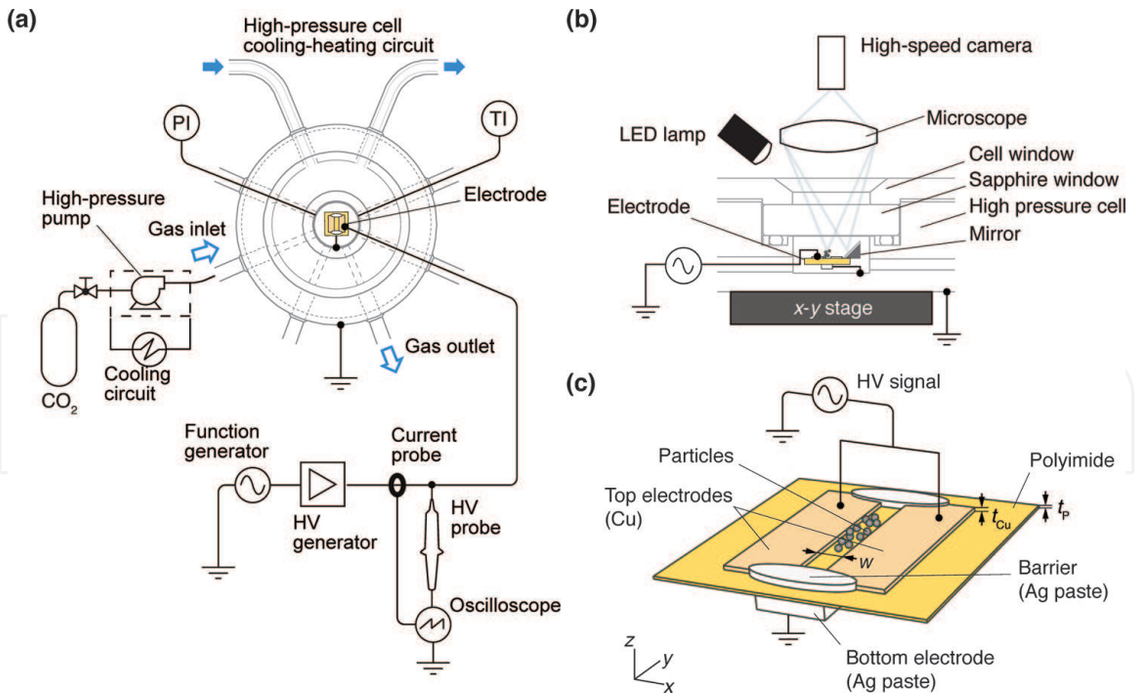

Figure 3.
Schematic of the experimental setup for the generation of the dusty plasmas in $scCO_2$: (a) top view, (b) side view, and (c) the electrodes (adapted from [23], © IOP Publishing Ltd., all rights reserved).

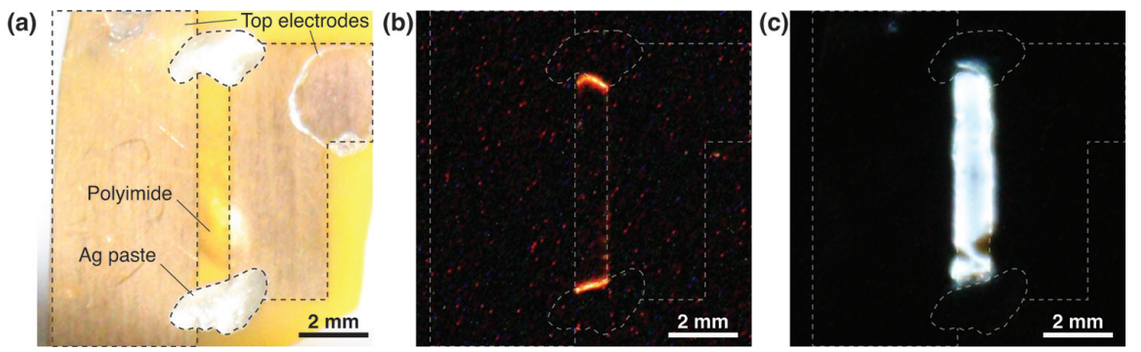

Figure 4.
Images of electrodes (a), surface DBD in field-emitting regime in $scCO_2$ (b), and in standard-regime in CO_2 at 1 atm (c) (adapted from [23], © IOP Publishing Ltd., all rights reserved).

2.2 Generation of dusty plasmas in $scCO_2$

Figure 4 shows photos of the electrodes and the plasmas generated with them without microparticles placed. **Figure 4a** shows photos of the electrodes whose etching width was 670 μm. **Figure 4b** shows the plasmas generated in $scCO_2$ in the field-emitting regime. The red luminescence is consistent with the previous optical emission spectroscopy measurement, which suggests that this is induced by electron-neutral bremsstrahlung [18]. **Figure 4c** shows the plasmas generated at atmospheric pressure in the standard regime, whose luminescence was blue or white, which might be derived from atomic emission.

In the experiments with particles, the particles in the etched region of the electrodes started to move intensely near the electrode surface when the voltage of ~3.0 $kV_{p\text{-}p}$ with a frequency of 10 kHz was applied, while many particles adhered to the Cu film and the Ag pastes, as shown in **Figure 5**. The moving particles were possibly electrically charged and accelerated by the AC electric field. When the frequency was decreased to 1 kHz, several particles floated above the electrodes, as shown **Figure 6**. **Figure 6a** shows the top view, where it is confirmed that the

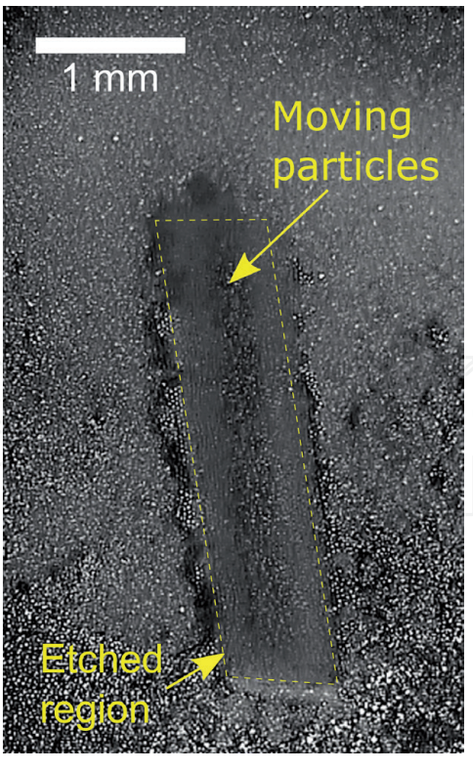

Figure 5.
Image of the particles moving near the electrode surface.

particles aligned at the center of the etched region. The particles showed motion along the electrode edge, whose direction is indicated in **Figure 6a**. **Figure 6b** shows the side view. The particles were levitated at a height of 500 μm or more above the electrode surface. These phenomena could be observed in the condition of high-pressure gaseous, liquid, and supercritical CO_2. It was considered that the particles levitated after the applied frequency was lowered, because the particles are likely to follow the AC electric fields with lower frequency, which is discussed in detail later.

2.3 Numerical simulations of the particle motion

The equation of motion of charged particles in $scCO_2$ shown below was numerically solved:

$$m\frac{d^2z}{dt^2} = -mg + \rho Vg - k\frac{dz}{dt} + QE(z)\sin 2\pi ft \quad (1)$$

where m is the particle mass, z is the height of the particle from the electrode surface, t is the time, g is the gravitational constant, ρ is the mass density of CO_2, V is the volume of the particle, $k = 6\pi\eta r$ is the viscous drag coefficient, η is the viscosity of CO_2 and was obtained from the NIST database [25], r is the radius of the particle, Q is the particle charge, $E(z)$ is the electric field along z, and f is the applied frequency. $E(z)$ was obtained from the derivative of the electric potential calculated with the finite-element method using freely available software [26]. **Figure 7** shows the contour map of the electric potential near the electrodes with an applied voltage of 5 kV. Here, z is defined as the opposite direction of the gravitational force so that z = 0 corresponds to the electrode surface (the surface of the polyimide film in the etched region); x and y are defined as the direction parallel to the electrode surface, as indicated in **Figure 6**. **Figure 7** is the cross-sectional view of the electrodes in

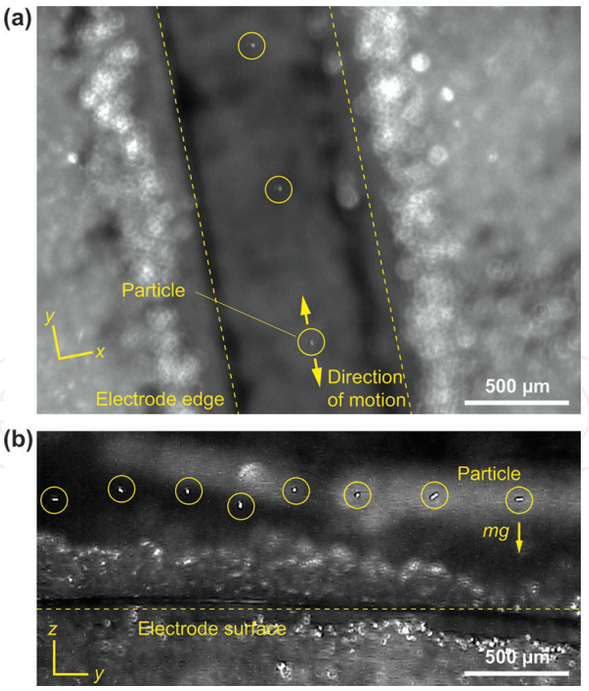

Figure 6.
Images of particles aligned above the electrodes: (a) top view and (b) side view (adapted from [23], © IOP Publishing Ltd., all rights reserved).

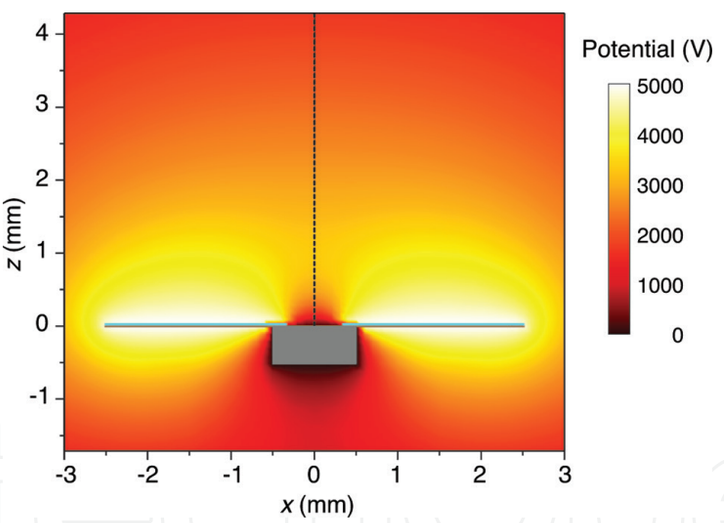

Figure 7.
Contour map of the calculated electric potential near the electrodes with the applied voltage of 5 kV (adapted from [23], © IOP Publishing Ltd., all rights reserved).

the x-z-plane, and it is assumed for the calculation that the y-direction is infinitely extended. The position of interest is $x = 0$, where the particles aligned in the experiments. **Figure 8** shows the electric field along the z-direction $E(z)$ at $x = 0$. However the applied voltage is large, the absolute value of $E(z)$ is the highest at the electrode surface, and $E(z)$ becomes 0 at a certain height from the electrode surface, above which its sign becomes inverted.

The time evolution of the height from the electrode surface of the charged particle is shown in **Figure 9**. The condition is $scCO_2$, where the pressure is 8.07 MPa, temperature is 305.8 K, density is 0.641 g cm^{-3}, product of particle charge and peak voltage QU is $1.5 \times 10^5 e$ C kV, and applied frequency is 1.0 kHz.

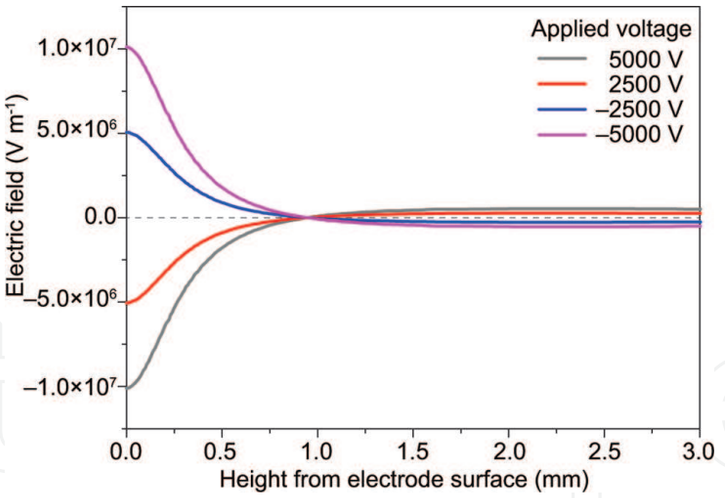

Figure 8.
Electric field along z-direction for each applied voltage at x = 0, which is indicated by the dotted line in **Figure 7** *(adapted from [23], © IOP Publishing Ltd., all rights reserved).*

Three types of initial condition were tried for the calculation. The first one was the particle on the electrode surface ($z = 0$), the second was the particle at the potential valley ($E_z = 0$), and the last was the particle staying far from the electrode surface ($z = 3$ mm). Whichever initial condition was used, the particle settled at a certain z after enough time passed. **Figure 10** shows the magnified graph of the particle position with the initial condition $z = 0$. The particle moves upward very rapidly and reaches the maximum height within 10 ms. After that, it moves downward and settles at z between 650 and 660 μm. The inset shows the particle motion after the settlement. The particle shows oscillation with an amplitude of 5 μm and a period of 1 ms. The frequency of this oscillation corresponds to the applied AC frequency. This oscillation is too small and fast to visualize in the scale of **Figure 9**.

2.4 Estimation of charge and coulomb coupling parameter

The equilibrium positions of the particle were plotted against the product of the particle charge and the applied peak voltage QU for each AC frequency, as shown in **Figure 11**. The condition is the same as the calculation shown in **Figure 9** except for QU. The error bars indicate the oscillation amplitudes. The equilibrium height increases with increasing QU and lowering the AC frequency. A higher QU means stronger electric fields applied on the particle. The particle is likely to follow the AC field with a lower frequency, which is also confirmed by the fact that the oscillation amplitudes are larger for the lower frequency. The experimental result that the particles levitated after the lowering of the AC frequency can be explained by this analysis. The plots in **Figure 11** have important implications for the particle charge. In fact, the particle charges can be estimated from the measured height of the particle from the electrode surface. The range of the particle charge estimated from the experimental results was on the order of $(10^4–10^5)e$ C. The particle charge is reported to be $(1–3) \times 10^3 e$ C with the orbital motion limited theory [27], $(10^3–10^5)e$ C with the analysis of particle motion [28], and on the order of $10^6 e$ C with Faraday cup measurement [29]. Therefore, the estimated particle charge is considered to be of a reasonable order. These analyses lack the information on the sign of the particle charges, although it is a common understanding that particles in a discharge plasma get negatively charged because

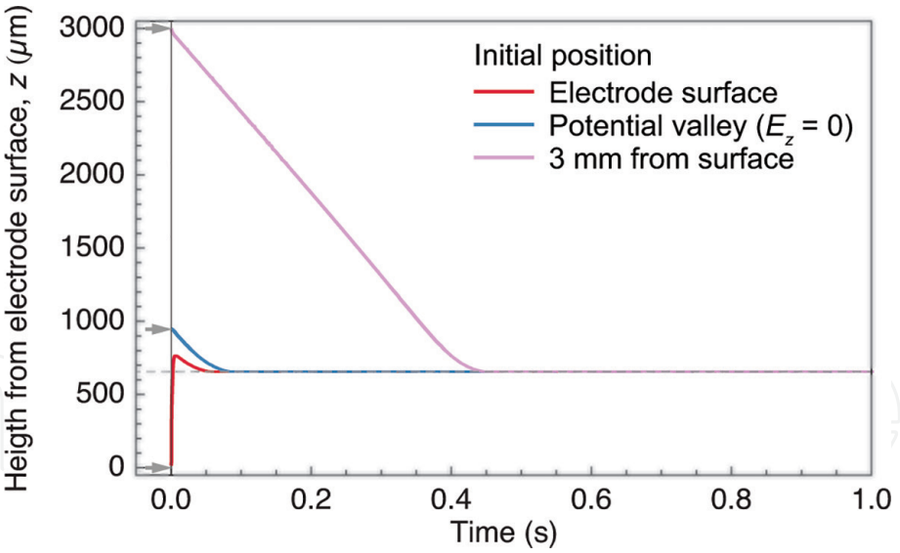

Figure 9.
Calculated time evolution of the height of charged particle for each initial position (adapted from [23], © IOP Publishing Ltd., all rights reserved).

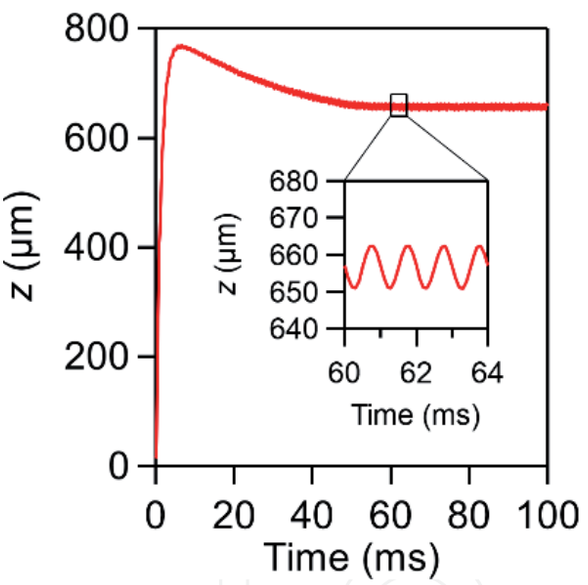

Figure 10.
Magnified graph of **Figure 9** *for the initial position of electrode surface (data adapted from [23]).*

of the higher mobility of electrons. Therefore, DC offset was applied to clarify the sign. **Figure 12** shows the changes of the particle positions with DC offset. When negative bias was applied, the particle moved downward. Meanwhile, the particle moved upward with the positive offset. This behavior is consistent with the numerical simulation results for the negatively charged particle, as shown **Figure 13**. The average position of the particle is 820 μm with the applied offset of +50 V and 656 μm without offset. It is considered that the particles get negatively charged by the discharges in $scCO_2$ because of the flux of the electrons emitted from the electrodes by field emission.

The kinetic energy of a particle was estimated with high-speed imaging. The motion along the y-direction is shown in **Figure 6a**. The movie was recorded with a frame rate of 125 fps and a duration of 3.848 s. **Figure 6a** is captured from this movie. The velocities of three particles were in the range of (1.4–2.1) × 10^2 μm s^{-1},

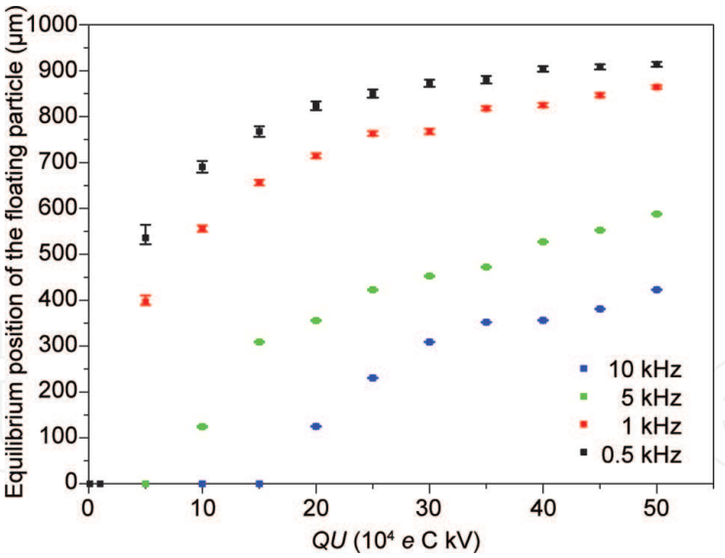

Figure 11.
Equilibrium position of the particle against the product of particle charge and applied peak voltage QU (© IOP Publishing Ltd., all rights reserved).

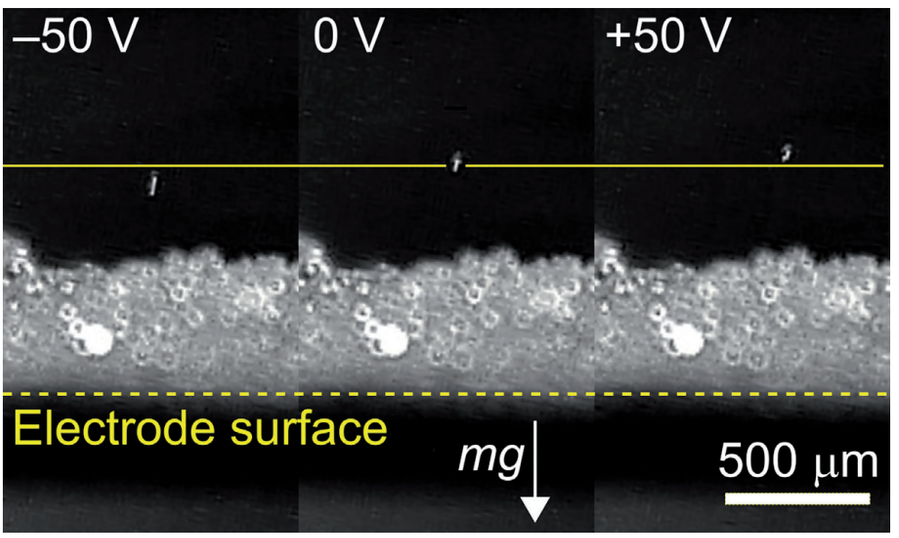

Figure 12.
Change in the height of the particle by applying DC offset.

from which the kinetic energy was (1.8–4.5) × 10^4 K. Assuming that the interparticle distance was 700 mm and the particle charges were $-(10^4–10^5)e$ C, this system had a Coulomb coupling parameter on the order of $10^2–10^4$ and is considered to be a strongly coupled plasma.

To the authors' knowledge, this is the first report on the formation of strongly coupled dusty plasmas in a dense medium. Almost all the reports employ RF plasmas in a vacuum to generate dusty plasmas. There are a few reports on the strongly coupled dusty plasmas generated in thermal plasmas under atmospheric pressure, where CeO_2 particles get positively charged by the thermal emission of electrons [30]. No other studies on the generation of dusty plasmas in a dense medium, such as high-pressure gas, liquid, and SCF, have been reported. Furthermore, this study is the first report on the formation of plasma crystals using DBD. Conventional plasma crystals have been formed in DC or RF glow discharge with metallic electrodes. DBD, which is usually employed for generating low-temperature plasmas under relatively high pressure, such as atmospheric-pressure plasmas, has not been used for plasma crystals up to now.

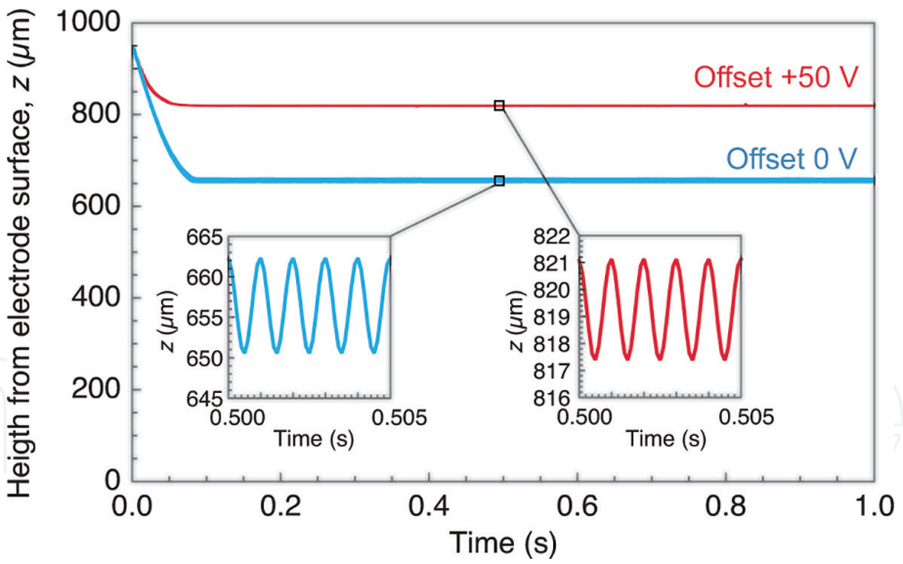

Figure 13.
Time evolution of the height of the particle with and without DC offset (© IOP Publishing Ltd., all rights reserved).

3. Pseudo-microgravity environment for dusty plasmas in $scCO_2$

The charging of particles by discharge in $scCO_2$ was clarified, and the particle charges were successfully estimated, as shown in the previous section. However, the microparticles used in Section 2 were so heavy that the pseudo-microgravity environment was hardly realized. In this section, lighter resin particles were used. Compensation for gravitational force by buoyancy was confirmed by controlling the balance between gravitational force and buoyancy, suggesting the formation of a microgravity environment for dusty plasmas in $scCO_2$. The formation behavior was analyzed by the estimation of the Coulomb coupling parameter.

3.1 Experimental approach

The experimental setup and the simulation method were basically the same as in Section 2. The width of the etched region of the upper electrodes was 2.7 mm. The particles employed were lighter. Their mass density was 0.5 g cm^{-3}. The experimental conditions were $mg > \rho Vg$ for condition (a); $mg \sim \rho Vg$ for conditions (b), (c), and (d); and $mg < \rho Vg$ for condition (e) as shown in **Figure 14**. The density of CO_2 for each condition is shown in **Figure 14**. The temperature was set to 31.7–32.1°C, slightly higher than the critical temperature of CO_2 (31.1°C). Condition (a) has a pressure of 6.92 MPa, where CO_2 is gaseous, and its density is lower than that of the particle. CO_2 is a supercritical condition in conditions (b), (c), (d), and (e).

3.2 Generation of dusty plasmas in $scCO_2$ with varying density of media

As in the previous section, several particles got levitated and trapped above the electrodes after the AC frequency was decreased. The applied AC voltage was 5 $kV_{p\text{-}p}$, and the frequency was initially 10 kHz and decreased to 155 Hz. **Figure 15i** is the side view of the particle arrangement with condition (a). The particles formed a single-layer structure. However, when the CO_2 density was controlled in condition (c), particles were arranged in the gravitational direction, as shown in **Figure 15ii**. The particles were also arranged in the *x-y* (horizontal)-plane, as shown in **Figure 16**, which confirmed the 3D arrangement of particles resulting from the

compensation of the gravity. It was observed that some particles exchanged their positions with their neighbors. Furthermore, the structure is not periodic—in other words, it is liquid-like. The particles formed a single- or double-layer structure with condition (e), as shown in **Figure 15iii**. Of all the experimental conditions, 3D structures were formed in the pseudo-microgravity conditions (b), (c), and (d). The window of the density of CO_2 for the formation of 3D plasma crystals was found to be ±0.2 g cm^{-3} compared with that of the particles.

The particles showed oscillation in the gravitational direction with a frequency equal to the applied AC frequency. In condition (c), the particles staying above and below the dashed line indicated in **Figure 15ii** showed oscillations antiphase to each other, the amplitudes of which were 20 and 60 μm, respectively.

3.3 Numerical simulations for pseudo-microgravity condition

To analyze the motion of a particle in the experimental conditions, Eq. (1), explained in the previous section, was applied. The initial position of the particle was set to $z = 0$. The particle charge was assumed to be $-7 \times 10^4 e$ C based on the results explained in the previous section. **Figure 17** shows the calculated time evolution of a particle for each density of CO_2. The particle starts to move upward after $t = 0$ and reaches a steady height in all conditions. The inset shows the magnified graph with the particles staying at a steady position. The steady height increases with increasing CO_2 density and approaches the position where the electric field is zero at any time with ρVg approaching mg. Additionally, the particles oscillate with applied AC frequency. The oscillation amplitude was smaller when $mg = \rho Vg$ than in any other condition.

3.4 Estimation of Coulomb coupling parameter

For the estimation of the Coulomb coupling parameter, the kinetic energies of both the oscillation and thermal motion of the particles were taken into consideration, instead of the thermal energy. The latter was assumed to be the same as the temperature of the chamber because of the small heat generation in the surface DBD in the field-emitting regime [18]. The oscillation energy was calculated as $mA^2(2\pi f)^2/2$ on the supposition that the oscillation is harmonic, where A is the

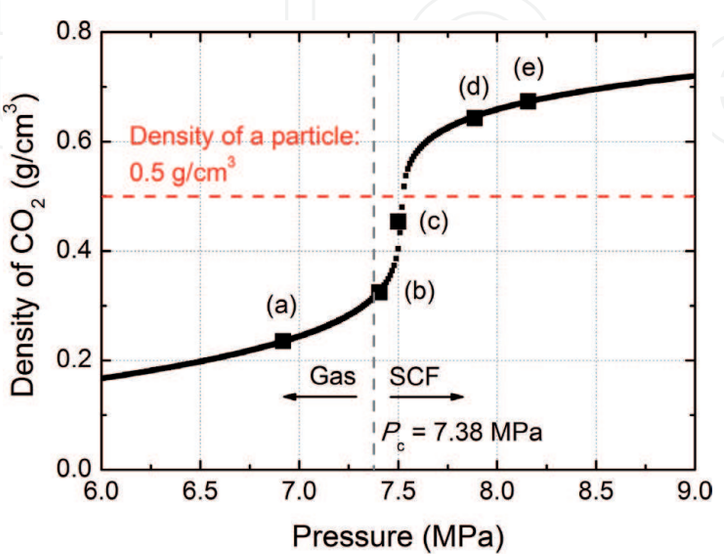

Figure 14.
Dependence of CO_2 density on pressure: the density of the particle is indicated by the red broken line, and the experimental conditions (a)–(e) are plotted (reprinted from [24], with the permission of AIP Publishing).

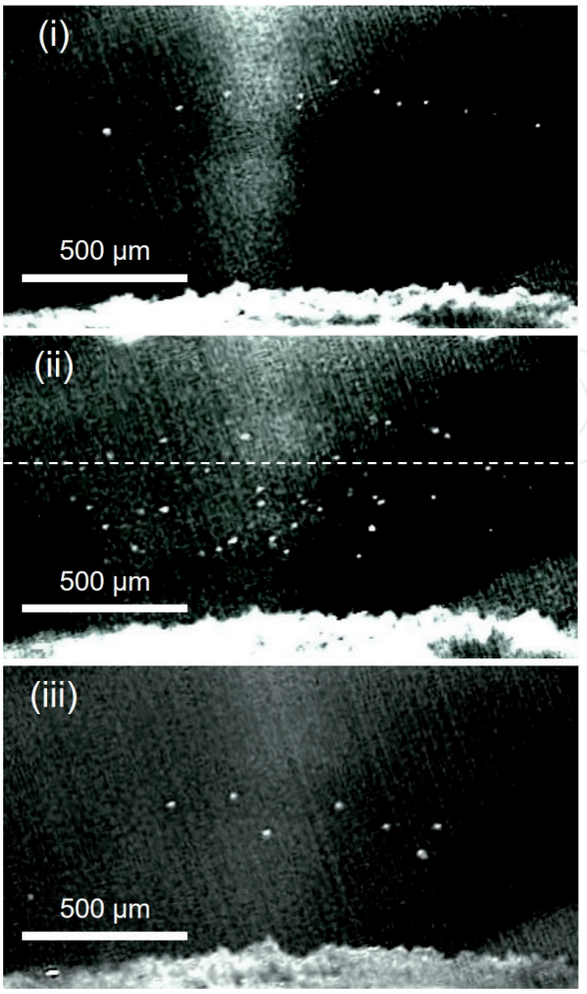

Figure 15.
Side view of the trapped particles above the electrodes with the condition of mg > ρVg (i), mg = ρVg (ii), and mg < ρVg (iii) (reprinted from [24], with the permission of AIP Publishing).

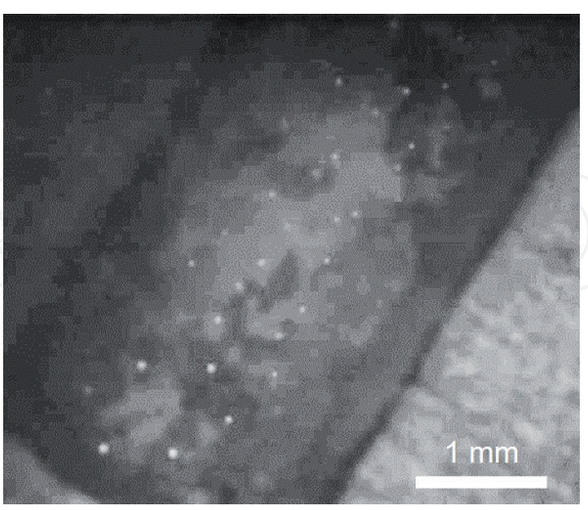

Figure 16.
Top view of the trapped particles with the condition of mg = ρVg (reprinted from [24], with the permission of AIP Publishing).

oscillation amplitude of a particle. The dependence of the oscillation amplitude on CO_2 density is shown in **Figure 18a**. The amplitude has the minimum value when $mg = \rho Vg$, as suggested in **Figure 17**. The calculated oscillation energy was in the range of 9.4×10^{-24}–3.4×10^{-15} J, while the thermal random motion energy

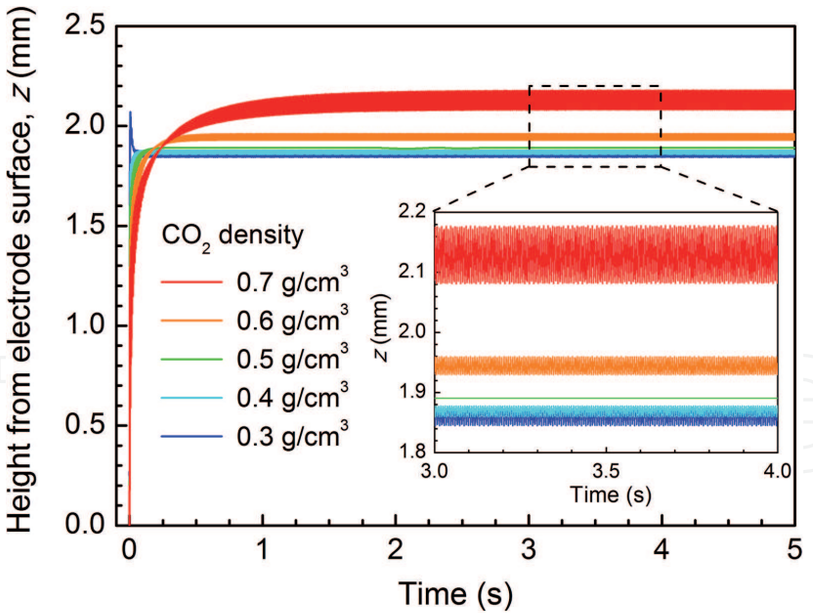

Figure 17.
Calculated time evolution of the height of the particle with each CO_2 density (reprinted from [24], with the permission of AIP Publishing).

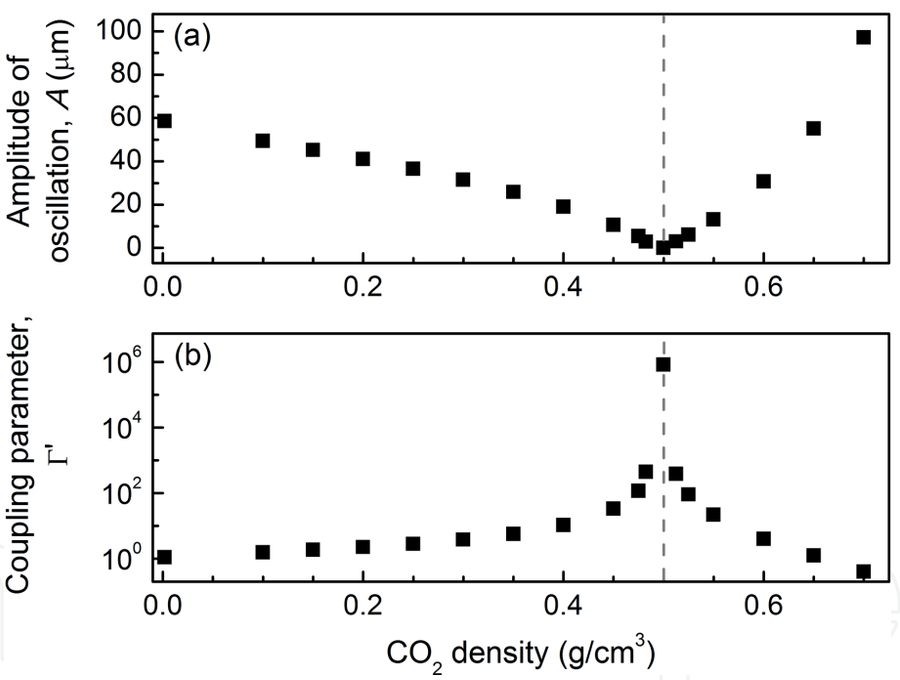

Figure 18.
Dependence of the amplitude of the oscillation of the particle (a) and the Coulomb coupling parameter (b) (reprinted from [24], with the permission of AIP Publishing).

was 4.2×10^{-21} J. The particle charge and the interparticle distance are assumed to be $-7 \times 10^4 e$ C and 250 μm, respectively. **Figure 18b** shows the dependence of the Coulomb coupling parameter on CO_2 density. The coupling parameter shows the maximum value when $mg = \rho Vg$ because of the suppression of the oscillation energy. The coupling parameter is possibly enhanced with the aid of the gravity compensation by buoyancy. The calculated Coulomb coupling parameter for condition (c), which is the closest to the condition with $mg = \rho Vg$ in this study, is less than the previously reported criterion for the transition from liquid to solid ($\Gamma > 170$) [31–33], which is consistent with the observation of liquid-like behavior.

4. Outlook for dusty plasmas in SCF

4.1 Pseudo-microgravity condition

The pseudo-microgravity conditions for dusty plasmas provide the opportunity to study collective phenomena without any anisotropy. **Figure 19** summarizes this study and shows its further application, as discussed below. Microgravity experiments using huge, expensive pieces of apparatus, such as a space station, largely limit the number of experimental trials. Therefore, some exciting discoveries have been possibly missed.

One of the unexplored phenomena is the rotation of a particle on its own axis, which was suggested by Sato at a workshop held at Tohoku University in 2014 [34]. Before going into details, the similarity between dusty plasma physics and solid-state physics should be considered. It is useful for finding novel phenomena in dusty plasmas to learn from solid-state physics. The idea of plasma crystals is similar to that of strongly correlated electron systems in a solid. In commonly used plasmas, ions and electrons have a large kinetic energy (=0.01–1 eV) and small interparticle electrostatic energy owing to small particle charge and large interparticle distance (low number density), which results in a very small Coulomb coupling parameter. Therefore, strongly coupled plasmas ($\Gamma > 1$) can hardly be realized. The introduction of dust particles changes that situation. The particles collect many electrons and have a large electric charge. In addition, they have a large mass to prevent acceleration and small kinetic energy, which results in a large Coulomb coupling parameter and possible realization of strongly coupled plasmas. Meanwhile, electron-electron interaction has great importance in the field of solid-state physics. The conducting electrons in a simple metal, such as Cu and Al, have no or weak interactions between electrons and can move freely. Some transition metal oxides and rare-earth oxides possibly show the localization of electrons and insulating behavior because of large electrostatic repulsion between electrons, even if they have a partially filled electron band in a simple band picture. The so-called Mott insulator shows various phenomena, such as a metal-insulator transition, magnetic transition, and superconducting transition with or without applying temperature change, chemical doping, and so on. Mott insulators have been one of the most extensively studied subjects [35]. There seem to be similarities between dusty plasmas and a strongly correlated electron system, given that, in both cases, novel ordered phases appear with strengthening of the interactions, which was considered to be ignorable. Some of the exciting phenomena observed in a strongly correlated electron system possibly emerge in dusty plasmas in a similar manner.

One of the examples might be the rotation of a particle on its own axis, which is like the spin of an electron. The positions of particles in dusty plasmas have been successfully tracked; however, there are no reports on their rotation to the authors' knowledge. It may be difficult to observe because the particle size is small (several tens of micrometers at largest). Larger particles are likely to sink because they are heavy. However, particle size does not matter in microgravity experiments. Using millimeter-sized particles possibly reveals the details of particle motion. The pseudo-microgravity condition can also make experiments with larger particles possible, because particle size does not matter so long as the density of the media is matched to that of the particle.

The applicability of heavier particles in microgravity experiments provides opportunities to use functional oxide or metal particles. Many studies on dusty plasmas employ resin particles, which possess no notable functional properties except for lightness. Using functional particles might make dusty plasmas

functional: susceptible to a magnetic field using magnetic particles [36], photocatalytic using photocatalyst particles, and so on. Such functional dusty plasmas are attractive as a functional fluid whose flow and reactivity can be controlled by a magnetic field or light irradiation. In addition, functional particles, such as magnetic or ferroelectric ones, are expected to show the interparticle interaction via such properties. Such interaction yields intentionally introduced anisotropy, which possibly causes the emergence of the crystal structures that still have not been observed in dusty plasmas or novel phase transitions.

4.2 Dusty plasmas in dense media

Another aspect of dusty plasmas in SCF is a density of media higher than in dusty plasmas in vacuum and lower than or comparable to that in colloidal dispersion. In colloidal dispersion, interparticle interaction is mediated via solvent flow, unlike in the case of dusty plasmas, where particles interact directly with each other via electrostatic force. Dusty plasmas in SCF are considered to be placed at the transient region, as shown in **Figure 20**. Changes of the mode of the interactions might be observable in dusty plasmas in SCF.

In this study, the existence of electrons and ions in the region of trapped particles and their screening effects were ignored. That region is somewhat far from surface

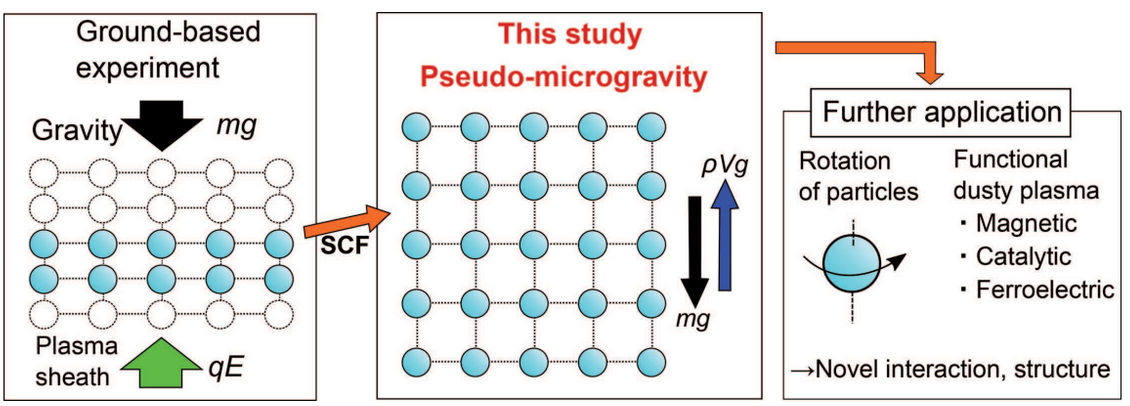

Figure 19.
Overview and further application of this study.

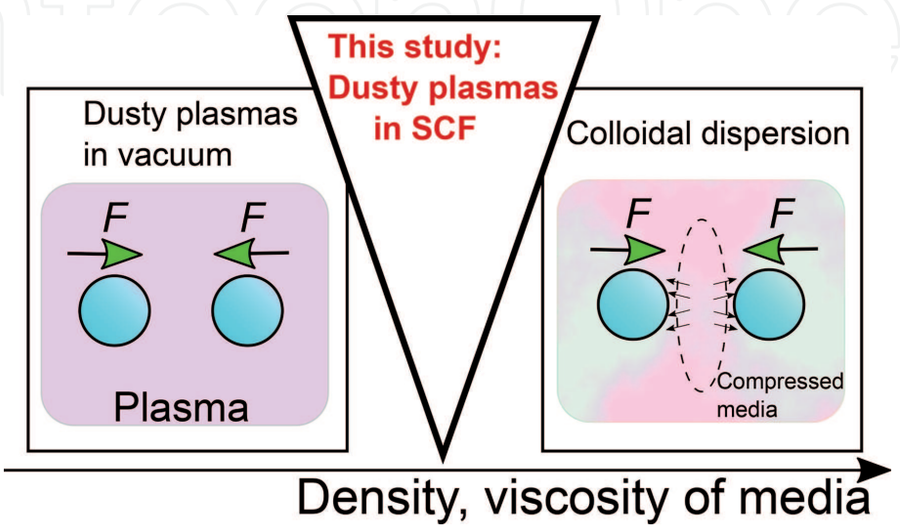

Figure 20.
Interparticle interaction modes in dusty plasmas in vacuum, colloidal dispersion, and the transient region, dusty plasmas in SCF.

DBD; therefore, there seem to be few electrons and ions when SCF is taken as a high-pressure gas, because their lifetime is too short under high pressure owing to frequent collisions. However, SCF also has a liquid-like characteristic. Solvated ions in a liquid have a long lifetime, and it was reported that electrons generated by discharge plasmas can be solvated [37]. The lifetime of ions and electrons in SCF is possibly so long that they can reach where the particles stay. The behaviors of the electrons and ions in plasmas generated in SCF are still not fully understood. Further analysis of the interparticle interaction in dusty plasmas in SCF could serve as a probe to clarify it.

5. Conclusion

Plasma crystals, realized in dusty plasmas, provide opportunities to study statistical phenomena and lattice dynamics in a crystal. However, in ground-based experiments, gravity imposes a large anisotropy on plasma crystals, which results in their 2D structure. This study on the dusty plasmas in SCF aimed at overcoming the problems caused by gravity that hinder research on dusty plasmas. The particles were successfully electrically charged by the surface DBD in $scCO_2$. The estimation of the particle charge and the analysis of the particle motion confirmed the formation of strongly coupled plasmas. With the density of $scCO_2$ matched to that of particles, which means a pseudo-microgravity condition for the particles, 3D-ordered structures were successfully formed. The pseudo-microgravity conditions provide opportunities to find novel phenomena and to develop functional dusty plasmas. In addition, the dusty plasmas in SCF can be considered as the intermediate phase between dusty plasmas in vacuum and colloidal dispersion. SCF is left largely unexplored with regard to the media for the generation of strongly coupled plasmas. Our pioneering works has been opening a novel field of strongly coupled plasmas.

Acknowledgements

This work was supported financially by a Grant-in-Aid for Scientific Research on Innovative Areas (Frontier Science of Interactions between Plasmas and Nanointerfaces, Grant No. 21110002) and the Grant-in-Aid for Challenging Exploratory Research (Grant No. 15K13389) from the Ministry of Education, Culture, Sports, Science, and Technology (MEXT) of Japan. We would like to thank Sekisui Chemical Co., Ltd. for providing us the fine resin particles (HB-2051) used in this study. One of the authors of this chapter, K.T., would like to give special thanks to Professor O. Ishihara (Chubu University) for his valuable suggestions and encouragement.

Conflict of interest

The authors declare no conflict of interest.

Author details

Yasuhito Matsubayashi[1*], Noritaka Sakakibara[2], Tsuyohito Ito[2] and Kazuo Terashima[2]

1 Advanced Coating Technology Research Center, National Institute of Advanced Industrial Science and Technology, Tsukuba, Ibaraki, Japan

2 Department of Advanced Materials Science, Graduate School of Frontier Sciences, The University of Tokyo, Chiba, Japan

*Address all correspondence to: y-matsubayashi@aist.go.jp

References

[1] Bragg WL, Nye JF. A dynamical model of a crystal structure. Proceedings of the Royal Society of London. Series A: Mathematical and Physical Sciences. 1947;**190**:474-481

[2] Pieranski P. Two-dimensional interfacial colloidal crystals. Physical Review Letters. 1980;**45**:569

[3] Hayward RC, Saville DA, Aksay IA. Electrophoretic assembly of colloidal crystals with optically tunable micropatterns. Nature. 2000;**404**:56

[4] Ikezi H. Coulomb solid of small particles in plasmas. Physics of Fluids. 1986;**29**:1764-1766

[5] Ichimaru S. Strongly coupled plasmas: High-density classical plasmas and degenerate electron liquids. Reviews of Modern Physics. 1982;**54**:1017

[6] Slattery WL, Doolen GD, DeWitt HE. Improved equation of state for the classical one-component plasma. Physical Review A. 1980;**21**:2087

[7] Thomas H, Morfill GE, Demmel V, Goree J, Feuerbacher B, Möhlmann D. Plasma crystal: Coulomb crystallization in a dusty plasma. Physical Review Letters. 1994;**73**:652

[8] Hayashi Y, Tachibana K. Observation of Coulomb-crystal formation from carbon particles grown. Japanese Journal of Applied Physics. 1994;**33**:L804

[9] Chu JH, Lin I. Direct observation of Coulomb crystals and liquids in strongly coupled rf dusty plasmas. Physical Review Letters. 1994;**72**:4009

[10] Morfill GE, Thomas HM, Konopka U, Rothermel H, Zuzic M, Ivlev A, et al. Condensed plasmas under microgravity. Physical Review Letters. 1999;**83**:1598

[11] Nefedov AP, Morfill GE, Fortov VE, Thomas HM, Rothermel H, Hagl T, et al. PKE-Nefedov*: Plasma crystal experiments on the International Space Station. New Journal of Physics. 2003;**5**:33

[12] Arp O, Block D, Piel A, Melzer A. Dust Coulomb balls: Three-dimensional plasma crystals. Physical Review Letters. 2004;**93**:165004

[13] Arp O, Block D, Klindworth M, Piel A. Confinement of Coulomb balls. Physics of Plasmas. 2005;**12**:122102

[14] Samsonov D, Zhdanov S, Morfill G, Steinberg V. Levitation and agglomeration of magnetic grains in a complex (dusty) plasma with magnetic field. New Journal of Physics. 2003;**5**:24

[15] Zhu J, Li M, Rogers R, Meyer W, Ottewill RH, Russel WB, et al. Crystallization of hard-sphere colloids in microgravity. Nature. 1997;**387**:883

[16] Ito K, Yoshida H, Ise N. Void structure in colloidal dispersions. Science. 1994;**263**:66-68

[17] Cansell F, Chevalier B, Demourgues A, Etourneau J, Even C, Pessey V, et al. Supercritical fluid processing: A new route for materials synthesis. Journal of Materials Chemistry. 1999;**9**:67-75

[18] Pai DZ, Stauss S, Terashima K. Field-emitting Townsend regime of surface dielectric barrier discharges emerging at high pressure up to supercritical conditions. Plasma Sources Science and Technology. 2015;**24**:25021

[19] Ivlev A, Hartmut LÃ, Morfill G, Royall CP. Complex Plasmas and Colloidal Dispersions: Particle-Resolved Studies of Classical Liquids and Solids. Singapore: World Scientific Publishing Company; 2012

[20] Stauss S, Muneoka H, Terashima K. Review on plasmas in extraordinary media: Plasmas in cryogenic conditions and plasmas in supercritical fluids. Plasma Sources Science and Technology. 2018;**27**:23003

[21] Stauss S, Muneoka H, Urabe K, Terashima K. Review of electric discharge microplasmas generated in highly fluctuating fluids: Characteristics and application to nanomaterials synthesis. Physics of Plasmas. 2015;**22**:57103

[22] Pai DZ, Stauss S, Terashima K. Surface dielectric barrier discharges exhibiting field emission at high pressures. Plasma Sources Science and Technology. 2014;**23**:25019

[23] Matsubayashi Y, Urabe K, Stauss S, Terashima K. Generation of dusty plasmas in supercritical carbon dioxide using surface dielectric barrier discharges. Journal of Physics D: Applied Physics. 2015;**48**:454002

[24] Sakakibara N, Matsubayashi Y, Ito T, Terashima K. Formation of pseudo-microgravity environment for dusty plasmas in supercritical carbon dioxide. Physics of Plasmas. 2018;**25**:10704

[25] Lemmon EW, Huber ML, McLinden MO. NIST standard reference database 23: NIST Reference Fluid Thermodynamic and Transport Properties Version; 9; 2010. p. 55

[26] Meeker D. Finite element method magnetics. FEMM; 4; 2010. p. 32

[27] Fortov VE, Khrapak AG, Khrapak SA, Molotkov VI, Petrov OF. Dusty plasmas. Physics-Uspekhi. 2004;**47**:447

[28] Fortov VE, Nefedov AP, Molotkov VI, Poustylnik MY, Torchinsky VM. Dependence of the dust-particle charge on its size in a glow-discharge plasma. Physical Review Letters. 2001;**87**:205002

[29] Walch B, Horanyi M, Robertson S. Measurement of the charging of individual dust grains in a plasma. IEEE Transactions on Plasma Science. 1994;**22**:97-102

[30] Fortov VE, Nefedov AP, Petrov OF, Samarian AA, Chernyschev AV. Particle ordered structures in a strongly coupled classical thermal plasma. Physical Review E. 1996;**54**:R2236

[31] Farouki RT, Hamaguchi S. Thermal energy of the crystalline one-component plasma from dynamical simulations. Physical Review E. 1993;**47**:4330

[32] Fortov VE, Molotkov VI, Nefedov AP, Petrov OF. Liquid-and crystallike structures in strongly coupled dusty plasmas. Physics of Plasmas. 1999;**6**:1759-1768

[33] Fortov VE, Ivlev AV, Khrapak SA, Khrapak AG, Morfill GE. Complex (dusty) plasmas: Current status, open issues, perspectives. Physics Reports. 2005;**421**:1-103

[34] Sato N. Private communication. Workshop in Tohoku University; 2014

[35] Imada M, Fujimori A, Tokura Y. Metal-insulator transitions. Reviews of Modern Physics. 1998;**70**:1039

[36] Block D, Melzer A. Dusty (complex) plasmas—Routes towards magnetized and polydisperse systems. Journal of Physics B: Atomic, Molecular and Optical Physics. 2019;**52**:63001

[37] Rumbach P, Bartels DM, Sankaran RM, Go DB. The solvation of electrons by an atmospheric-pressure plasma. Nature Communications. 2015;**6**:7248